Modelling of a Coupled PV and ITES Air Conditioning System Based on MWorks and its Operation Analysis for a Large High-speed Railway Station

Guo Zhang[1] Weihua Zhou[1] Xinhua Xu[1] Fei Guo[2] Liwei Tian[2]

[1]Department of building environment and energy engineering, Huazhong University of Science and Technology, China,{bexhu@hust.edu.cn}
[2]China Railway Siyuan Survey and Design Group Co., Ltd, China

Abstract

Large high-speed railway stations are major energy consumers with enormous cooling loads. Integrating distributed renewables such as photovoltaics (PV) offers new prospects for building decarbonization but brings challenges to system dispatch and economic optimization. This study evaluates operational modes of a coupled PV and ice thermal energy storage (ITES) air conditioning system to maximize economic benefits. A physical simulation model of the PV+ITES system including PV module, chiller module, pump module, ice storage tank module etc. was built in MWorks. Three operation modes are considered, and the yearly operation performances were simulated. Quantitative comparison shows Mode 3 (combining PV direct supply and nighttime off-peak ice storage via TOU tariffs) performs optimally, with an annual net operating cost of 2.852 million CNY and 27.53% cost saving vs. Mode 1 (independent PV grid-connection), providing practical references for large transportation hubs.

Keywords: PV, ITES system, Operation analysis, MWorks

1 Introduction

Large high-speed railway stations, characterized by massive floor areas and high occupant densities, exhibit immense air conditioning cooling loads (Chen et al. 2025). They are major energy consumers within the transportation infrastructure sector. The expansive roofs of these stations present significant opportunities for the large-scale deployment of rooftop PV systems in dense urban areas (Zhu et al. 2023). However, a spatio-temporal mismatch often exists between PV generation peaks and building cooling load peaks. Consequently, standalone grid-connected PV systems struggle to achieve complete self-consumption. In this context, integrating energy storage technologies has emerged as a crucial strategy to promote the effective application of renewable energy. ITES can convert surplus PV power or off-peak nocturnal electricity into ice for storage. During periods of peak power demand, the system discharges this cold energy to reduce the operating load of chillers (Dong et al. 2023). ITES not only smoothes PV output fluctuations and enhances the self-consumption rate, but also effectively facilitates peak shaving and load shifting for the power grid (Hillen et al. 2025).

The coordinated operation and dispatch of coupled renewable energy and storage systems face complexity challenges. These challenges primarily arise from strong multi-component coupling and nonlinear thermodynamic dynamics. To evaluate the operating strategies of such coupled systems, existing studies typically adopt two main approaches. The first approach relies on mathematical optimization algorithms to seek globally optimal dispatch commands. For example, Shi et al. (2022) developed a mixed-integer linear programming model for the coordinated optimization of storage and generation capacities in a coupled system. Onaolapo et al. (2021) employed an adaptive model predictive control algorithm for the optimal dispatch and economic evaluation of PV, wind power, and battery energy storage systems in microgrids. Cirocco et al. (2022) developed an advanced control and forecasting algorithm to cooperatively dispatch PV and latent heat thermal energy storage to respond to electricity prices and achieve peak shaving. However, these methods usually require highly linearized assumptions for key thermodynamic processes, such as the nonlinear heat transfer during ice phase change. This oversimplification frequently leads to significant performance deviations between theoretical optimums and actual engineering implementations (Hao et al. 2022).

The second approach emphasizes dynamic physical simulation. It focuses on the high-fidelity capture of the authentic, nonlinear transient behaviors of HVAC equipment and energy storage devices. Tang et al. (2023) constructed nonlinear physical models of ice coils and chillers based on heat transfer analysis, accurately reflecting dynamic phase-change processes and chiller degradation under varying conditions. Pinamonti et al. (2020) utilized TRNSYS to perform high-precision simulations of a coupled PV, heat pump, and thermal storage system to evaluate practical control strategies. Nonetheless, traditional physical simulation tools typically adopt a causal (signal-flow) modelling paradigm. When applied to multi-domain, dynamically changing energy systems,

these tools are often compelled to adopt idealized control assumptions to avoid convergence issues. Furthermore, they tend to neglect the dynamic hydraulic characteristics and reverse pressure feedback of the pipe network (Fan et al. 2021).

In contrast, the acausal modelling language Modelica provides a highly flexible and physically compliant virtual environment. By supporting object-oriented, modular modelling from the first principles of physics, Modelica significantly enhances the efficiency and intuitiveness of modelling complex systems (Lu et al. 2021). The Modelica Buildings library, developed by the International Building Performance Simulation Association , has established the authoritative position of acausal modelling in handling interdisciplinary building energy systems (Wetter et al. 2014). In recent years, numerous scholars have conducted pioneering explorations using Modelica in related fields. For instance, Hinkelman et al. (2022) achieved high-fidelity dynamic simulations of large-scale district cooling networks and their pipeline hydraulics using Modelica. Li et al. (2021) specifically developed and validated a high-precision physical model of an ice storage tank based on Modelica, accurately capturing the nonlinear transient phase-change heat transfer process. Furthermore, Chen et al. (2025) successfully applied such phase-change physical models to the dynamic performance evaluation of complex HVAC systems. Targeting broader application scenarios, recent studies have not only utilized Modelica to accomplish the reduced-order physical validation of large-scale thermal energy storage systems (Formhals et al. 2024), but also achieved rapid, high-fidelity transient simulations of phase-change storage materials at the building level (Menezes et al. 2026).

Therefore, taking a large high-speed railway station as the background, the primary objectives of this study are to: (1) construct a digital-physical model of the coupled PV-ITES air conditioning system based on the MWorks platform, aiming to simulate and predict its transient responses under various disturbances, including solar radiation, ambient temperature, and dynamic building loads; (2) quantitatively evaluate the actual operational performance and economic benefits of different operation modes through dynamic simulation analysis; and (3) quantify the economic response of each operational mode to dynamic grid electricity prices. This study can provide a reliable theoretical basis and robust data support for the subsequent formulation of system control strategies.

2 System Description

This study investigates a coupled PV and ITES air conditioning system in a high-speed railway station in a south china city. From an energy provision perspective, a 2.05 MWp distributed PV array is integrated with the 10 kV railway grid for self-consumption, effectively reducing grid reliance. From the cooling production and distribution perspective, the system employs a 25% ethylene glycol aqueous solution as the primary heat transfer medium.

The principle of the chilled water system is illustrated in Figure 1. The primary loop is hydraulically decoupled from the secondary chilled water network to the user terminal via a 6860 kW plate heat exchanger. This specific configuration ensures robust physical isolation while enabling efficient thermal exchange. The core equipment comprises a single dual-mode chiller (cooling capacity: 4219 kW in cooling mode, 2827 kW in ice-storage mode) alongside two base-load chillers (3164 kW each). Latent heat storage is accomplished through an array of 24 individual ice storage tanks, each boasting a capacity of 277 RTh. Furthermore, the fluid transport and heat rejection infrastructure is supported by two ethylene glycol pumps, four chilled water pumps, four cooling water pumps, and seven cooling towers.

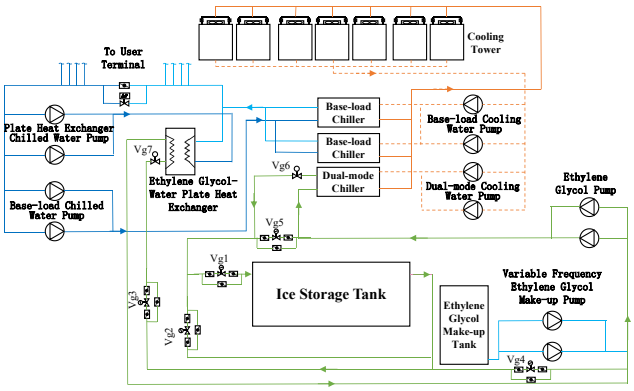


Figure 1. Principle of the chilled water system.

Furthermore, the ITES air conditioning system is configured with four primary operational modes: (1) ice-storage by the dual-mode chiller coupled with independent cooling by the base-load chillers; (2) combined direct cooling by both the dual-mode and base-load chillers; (3) joint cooling by all chillers combined with ice discharging; and (4) joint cooling by the base-load chillers and ice discharging. An automated control system seamlessly transitions among these modes based on real-time cooling loads, time-of-use (TOU) electricity tariffs, and predefined optimization strategies.

3 Modelling Based on MWorks

The coupled PV-ITES air conditioning system in a large high-speed railway station is an interdisciplinary engineering object that encompasses multiple physical domains, including thermodynamics, fluid dynamics, power electronics, and automated control. Modelica is a new-generation equation-based, acausal, and object-oriented modelling language. It can seamlessly bridge diverse physical fields, facilitating the convenient modelling of complex physical systems. MWorks serves as a comprehensive system-level design and simulation verification platform tailored for multi-domain industrial products. It fully supports the Modelica unified modelling specifica-

DOI
10.3384/ecp223371

tion and adopts a hierarchical modelling approach that mirrors real-world physical topologies thereby robustly underpinning model-based system engineering applications. Furthermore, MWorks provides a complete suite of capabilities, including system simulation modelling, compilation analysis, simulation solving and post-processing. It comprehensively covers the entire model-based system verification process.

To evaluate the dynamic operational performance of the aforementioned coupled PV and ITES air conditioning system, a system simulation model was developed in MWorks by using the Modelica language. Initially, physical models of core fundamental components, including the chiller model, the water pump model, the plate heat exchanger model, he cooling tower model, the PV system and the ice storage tank. They were established based on conservation laws and actual equipment performance parameters.

In the chiller model, a performance curve-based approach derived from the DOE-2.1 model is adopted. The dynamic available cooling capacity and the compressor power consumption are evaluated by applying correction functions for evaporator/condenser temperatures and part-load conditions. The core governing equations are expressed as the following formulas:

$$Q_{act} = Q_{ref} \times \mathrm{CAPFT}(T_{chw,o}, T_{cw,o}) \tag{1}$$

$$\begin{aligned} P_{act} = {} & P_{ref} \times \mathrm{CAPFT}(T_{chw,o}, T_{cw,o}) \\ & \times \mathrm{EIRFT}(T_{chw,o}, T_{cw,o}) \\ & \times \mathrm{EIRFPLR}(\mathrm{PLR}, T_{cw,o}) \end{aligned} \tag{2}$$

Where, Q_{act} and Q_{ref} denote the dynamic available and rated cooling capacities (W), respectively; P_{act} and P_{ref} are the actual and rated power consumptions (W); $T_{chw,o}$ is the leaving chilled water temperature from the evaporator (°C); and $T_{cw,o}$ is the leaving cooling water temperature from the condenser (°C). Both CAPFT and EIRFT are biquadratic polynomial functions of $T_{chw,o}$ and $T_{cw,o}$. Notably, the EIRFPLR is a biquadratic polynomial function of both the leaving condenser water temperature ($T_{cw,o}$) and the partial load ratio (PLR), effectively capturing the coupling degradation effects under off-design conditions.

In the water pump model, an empirical performance curve method is utilized. Based on the manufacturer's characteristic data at the nominal speed, the pump's transient pressure head and power consumption at any variable speed are dynamically calculated by using the affinity laws. The fundamental equations are defined as the following formulas:

$$H = r_N^2 \cdot s\left(\frac{\dot{V}}{r_N}, d\right) \tag{3}$$

$$P = r_N^3 \cdot s\left(\frac{\dot{V}}{r_N}, d\right) \tag{4}$$

Where, H is the pump head under specific operating conditions (Pa); P is the dynamic power consumption (W); r_N is the normalized speed (the ratio of actual speed to nominal speed); $\frac{\dot{V}}{r_N}$ represents the equivalent volumetric flow rate converted to the nominal speed condition; $s(...)$ represents the spline interpolation function based on the nominal performance curve data d.

In the plate heat exchanger model, the ε-NTU (effectiveness-NTU) method is implemented. Unlike simplified models with a constant overall heat transfer coefficient (UA), this model dynamically updates the UA value based on the real-time mass flow rates of the fluids to accurately reflect transient convective heat transfer behaviors. The core equations are expressed as the following formulas:

$$UA = \frac{1}{\frac{1}{hA_1} + \frac{1}{hA_2}} \tag{5}$$

$$Q_{flow} = \varepsilon \cdot Q_{max} \tag{6}$$

Where, UA is the dynamic overall heat transfer coefficient multiplied by the area (W/K); hA_1 and hA_2 are the products of the transient convective heat transfer coefficient and area for fluid 1 and fluid 2, respectively, which vary with real-time mass flow rates; Q_{flow} is the actual heat transfer rate (W); ε is the heat transfer effectiveness determined by NTU and flow regimes; Q_{max} is the theoretical maximum possible heat transfer rate (W).

In the cooling tower model, a physics-based grey-box approach based on Merkel's theory is adopted. The complex heat and mass transfer process is equivalently modeled as a counter-flow heat exchanger using the ε-NTU method, driven by the enthalpy difference between the saturated air at the water surface and the mainstream air. The actual heat transfer rate and the dynamic modification of the UA value under off-design conditions are expressed as the following formulas:

$$UA_e = UA_0 \cdot f_{wb} \cdot f_{air} \cdot f_{wat} \tag{7}$$

$$Q_t = \varepsilon \times C_{min} \times (T_{w,in} - T_{a,wb,i}) \tag{8}$$

Where, UA_e and UA_0 are the equivalent and nominal overall heat transfer coefficient-area products, respectively; f_{wb}, f_{air}, and f_{wat} represent the modification factors for current wet-bulb temperature, airflow, and water flow; Q_t is the actual total heat transfer rate of the cooling tower (W); ε is the effectiveness; C_{min} is the minimum heat capacity rate between air and water (W/K); $T_{w,in}$ and $T_{a,wb,i}$ are the entering water temperature and entering air wet-bulb temperature, respectively.

In the PV system model, the hourly power yield is dynamically calculated based on the global horizontal irradiance, installed capacity, and a comprehensive efficiency coefficient. The core governing equation is expressed as the following formula:

$$E_P = H_A \times \frac{P_{AZ}}{E_S} \times K \tag{9}$$

Where, E_P is the system power yield (kWh); H_A denotes the global horizontal irradiance (kWh/m^2); P_{AZ} is

the installed capacity (kWp); E_S is the standard test condition irradiance constant (defaulted to 1 kWh/m^2); K is the comprehensive efficiency coefficient, estimated between 81% and 85%.

In the ice storage tank model, a dynamic calculation method is employed based on the performance curves to reflect the transient thermodynamic characteristics during the charging and discharging processes. The rate of change of its core state parameter, the State of Charge (SOC), is governed by the following formula:

$$\frac{\mathrm{d}SOC}{\mathrm{d}t} = \frac{\dot{Q}}{H_f \cdot m_{ice,max}} \tag{10}$$

Where, SOC is a dimensionless number ranging from 0 to 1 (0 means completely melted, 1 means completely frozen); H_f is the latent heat of fusion of ice (J/kg); $m_{ice,max}$ is the maximum theoretical ice storage mass (kg); $\dot{Q}$ represents the transient heat transfer rate (W), which is positive during charging and negative during discharging.

Upon completing the construction of individual component models, these modules were organically coupled within the MWorks platform to establish the coupled system model, as depicted in Figure 2.

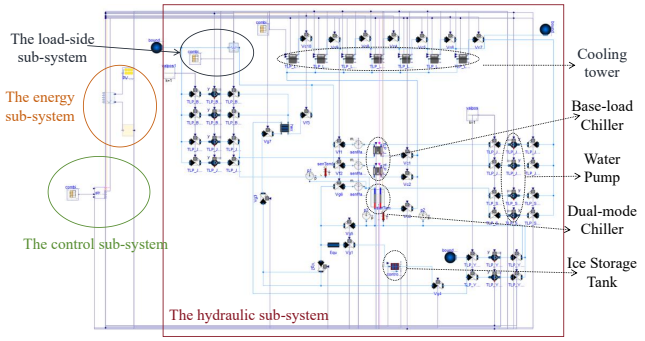


Figure 2. Simulation model of the coupled PV-ITES air conditioning system.

This coupled system model primarily comprises four sub-systems:

- The Hydraulic Sub-system: This constitutes the physical backbone of the entire model, mapping the actual piping topology and component interconnections. It encompasses all primary equipment, including the baseload chillers, dual-mode chillers, the ice storage tank, cooling towers, and the associated network of variable-speed pumps and valves.
- The Load Sub-system: It is represented by a simplified Air Handling Unit (AHU) model that calculates the required heat extraction based on building load profiles. This creates a closed-loop feedback mechanism, where the chilled water supply temperature from the hydraulic sub-system directly influences the AHU's heat exchange performance, ensuring a realistic representation of the interaction between the generation and demand sides.
- The Energy Sub-system: This module functions as the performance aggregator, responsible for quantifying the system's overall energy consumption and economic metrics. It dynamically calculates the total instantaneous power draw by summing the contributions from all major electrical components, including chillers, pumps, and cooling tower fans. Simultaneously, it accounts for the on-site PV power generation, computing the net grid electricity exchange that forms the basis for the subsequent economic analysis.
- The Control Sub-system: It receives dynamic boundary conditions as inputs, such as the building cooling load, PV generation forecast, and TOU electricity tariffs. Then it executes the predefined control strategies for each mode. Its outputs are the real-time control signals (e.g., on/off commands, temperature setpoints) that are dispatched to the actuators within the hydraulic sub-system.

4 Operation Modes

To evaluate economic performance and PV integration potential, this study compares three operational modes. Mode 1 is the baseline mode. In this mode, the ice storage system is disabled, building cooling loads are entirely met by conventional chillers, and all generated PV electricity is injected into the external grid. It is worth noting that while Mode 1 could theoretically utilize 100% pure water to improve hydraulic efficiency due to higher specific heat capacity, the simulation consistently maintained the 25% ethylene glycol properties across all modes to ensure a strictly unified physical baseline for economic comparison. To maximize hydraulic efficiency, the control logic strictly prioritizes the water-based base-load chillers. The dual-mode chiller remains on standby and is only activated as a supplementary backup during extreme peak load conditions. Thus, the majority of the cooling distribution benefits from the lower pump power consumption associated with pure water. Mode 2 utilizes direct cooling with PV self-consumption. The ice storage remains disabled, but the chillers prioritize local PV consumption, exporting surplus power to the grid and drawing from the grid only when encountering a power deficit. Mode 3 combines nighttime off-peak ice storage with daytime PV direct-supply. Deeply integrated with local TOU tariffs, this mode charges the ice storage using inexpensive grid electricity during nighttime off-peak valleys. During the daytime, it prioritizes PV output to drive base-load chillers in conjunction with ice discharging.

The 24-hour time-series dispatch logic of the system is illustrated in Figure 3. The different color blocks intuitively map the real-time operational boundaries of the system: blue for the idle state with no cooling load, red for direct cooling by conventional chillers, green for ice charging by the dual-mode chiller yellow for ice discharging from the storage tank.

DOI
10.3384/ecp223371

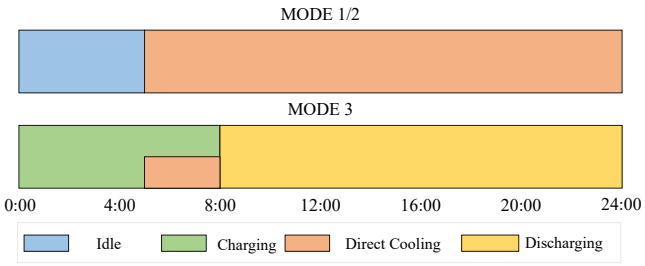


Figure 3. 24-hour time-series dispatch logic of the system.

During the direct cooling phase, a capacity allocation mechanism with hysteresis is embedded within the controller to ensure stable state transitions and prevent equipment oscillation caused by transient load fluctuations. The load threshold for activating the next sequential chiller is set at 95% of the total rated capacity of the currently running chillers, while the threshold for sequential shut-down is set at 80%. The specific staging sequence is as follows:

1. Base-load Chiller 1 operates as the primary active cooling source.
2. Base-load Chiller 2 is activated only when the real-time cooling load exceeds 95% of Chiller 1's rated capacity, and is shut down when the load drops below 80% of Chiller 1's rated capacity.
3. The dual-mode chiller (operating in cooling mode) is engaged only when the load exceeds 95% of the combined rated capacity of both base-load chillers, and is shut down when the load drops below 80% of this combined capacity.

During the ice discharging phase, the system prioritizes melting stored ice first, only activating regular chillers if the discharged cooling energy is insufficient to meet the instantaneous load.

In Mode 3, the periods from 5:00 to 8:00 AM operate as a parallel charging-and-cooling phase. The dual-mode chiller maintains ice-storage while the base-load chillers are sequentially activated to handle the initial building cooling loads. However, to guarantee cooling reliability, the system will take emergency action under extreme operating conditions. When the terminal load exceeds the maximum cooling capacity of the base-load chillers, it forcibly interrupts the ice-charging loop and smoothly switches the dual-mode chiller to the cooling state to respond to the peak load.

5 Results and Analysis

5.1 Evaluation Index

To systematically assess the operational characteristics, energy conversion efficiency, and grid interaction level of the PV system in the target scenario, the following key metrics are introduced to quantify the source-load matching performance.

The Self-Consumption Rate (SCR) denotes the proportion of PV-generated electricity that is directly consumed by the local load. It serves as a core indicator for evaluating the economic viability and source-load synergy of distributed PV systems. A higher SCR indicates that the majority of the PV generation is locally utilized, mitigating the economic degradation associated with high-tariff grid feed-in. The hourly self-consumption rate $SCR(t)$ is formulated as:

$$SCR(t) = \frac{E_{PV}(t) - E_{g,ex}(t)}{E_{PV}(t)} \times 100\% \tag{11}$$

Where, $E_{PV}(t)$ represents the PV power generation at time t (kWh); $E_{g,ex}(t)$ is the surplus PV power fed into the utility grid at time t (kWh).

Self-Sufficiency Rate (SSR) evaluates the system from the demand side. This metric intuitively reflects the local systems degree of independence from the main grid. A higher SSR implies enhanced system resilience against grid price fluctuations and potential supply instabilities. It represents the fraction of the local load demand directly fulfilled by the PV system:

$$SSR(t) = \frac{E_{load}(t) - E_{g,in}(t)}{E_{load}(t)} \times 100\% \tag{12}$$

Where, $E_{g,in}(t)$ is the power purchased from the external grid at time t due to insufficient PV output (kWh); $E_{load}(t)$ is the local load demand at time t (kWh).

The total self-consumption rate (SCR_{total}) and total self-sufficiency rate (SSR_{total}) can be derived by aggregating the aforementioned hourly metrics over a statistical period T (e.g., daily, monthly, or annually). Long-term evaluation metrics comprehensively reflect the overall energy efficiency of the system over the time dimension.

5.2 Dynamic Simulation Results and Analysis

Based on the annual dynamic simulation via the MWorks platform, the energy generation and consumption distributions under these three operation modes are presented in Table 1. In the baseline scenario (Mode 1), the annual grid electricity consumption reaches 4.90 GWh, while 2.33 GWh of PV generation is entirely exported to the grid, leading to zero local PV utilization. Following the introduction of the PV self-consumption mechanism (Mode 2), the system directly consumes 1.39 GWh of PV electricity, significantly reducing the grid electricity demand by 28.33%. Notably, the annual grid electricity consumption rebounds to 4.54 GWh in Mode 3, which is higher than in Mode 2. This rebound occurs because the load-shifting strategy transfers the heavy ice-storage load to the nighttime. During this period, the system not only relies entirely on the grid without any PV offset but also incurs the inherent thermodynamic efficiency degradation and auxiliary power consumption of the ice-storage cycle. Furthermore, this strategy results in a lower PV self-consumption of 1.16 GWh compared to Mode 2. This highlights a

critical trade-off: optimizing for price arbitrage in Mode 3 comes at the cost of reduced overall energy efficiency and lower direct PV utilization compared to a pure self-consumption strategy.

Table 1. Comparison of annual energy performance under 3 alternative modes.

Parameter	*Mode 1*	*Mode 2*	*Mode 3*
Grid electricity consumption (kWh)			
Annual total	4,902,029	3,513,142	4,536,961
Change vs. Mode 1	–	−1,388,888	−365,068
Reduction	–	28.33%	7.45%
PV self-consumption (kWh)			
Annual total	0	1,388,887	1,159,899
Increase vs. Mode 1	–	+1,388,887	+1,159,899
PV grid-export (kWh)			
Annual total	2,327,012	938,124	1,167,113
Change vs. Mode 1	–	−1,388,888	−1,159,899
Reduction	–	59.69%	49.84%

To deeply understand the thermodynamic behaviors and dispatch characteristics of different operation modes, a dynamic analysis on a typical day is indispensable. Although comprehensive dynamic simulations were conducted across various typical meteorological scenarios, including low, medium-high, and peak cooling load days. This study primarily presents the detailed transient results of the representative high-load day due to manuscript length constraints. The high-load scenario can effectively highlight the most rigorous operating conditions of the HVAC equipment, the maximum potential of PV energy utilization, and the critical thermodynamic scheduling conflicts among different operation modes.

To understand the thermodynamic characteristics that drive the energy distribution in different operation modes, Figure 4 provides a detailed breakdown of electricity consumption and the dynamic system Coefficient of Performance (COP). For Mode 1/2, the cooling demand is supplied directly by the chillers operating under conventional cooling conditions. The system COP remains relatively stable between 3.5 and 4.5 during the daytime operating hours (05:0023:00). In Mode 3, the integration of the ITES strategy alters the systems efficiency profile and load distribution. To accomplish the load-shifting objective, the dual-mode chiller operates extensively during the nocturnal hours (00:0007:00) to produce ice-storage. Due to the physical necessity of operating the evaporator at sub-zero temperatures during the ice-storage cycle, the compressor must overcome a larger temperature lift. Consequently, the system COP temporarily decreases to approximately 2.0 during the night. This inherent thermodynamic characteristic of latent heat storage explains the increased power consumption required to store cooling energy. During the morning ice-discharging phase (08:0010:00), the chillers are deactivated and the stored latent heat is released to meet the building's demand, with only the auxiliary pumps consuming power. During this period, the system achieves a high system COP (peaking at approximately 17.5).

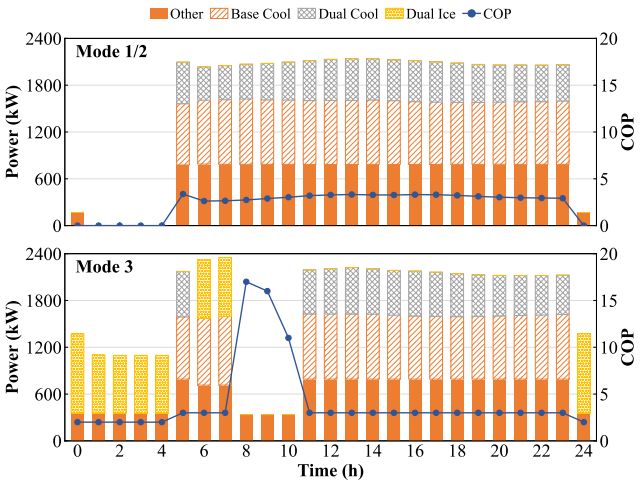


Figure 4. Detailed electricity consumption breakdown and the system COP on a typical high-load day.

Figure 5 illustrates the hourly electricity consumption breakdown alongside the SSR. In Mode 2, the system's dynamic electrical load follows a conventional bell-shaped curve, aligning seamlessly with the daytime cooling demand. Consequently, its SSR maintains a robust level during the daytime, peaking at 72% around 13:00, which effectively reduces peak-hour grid reliance. In contrast, Mode 3 reshapes the load profile to leverage off-peak electricity tariffs. Massive ice-storage loads are shifted to the nighttime. As depicted by the towering right bars in Figure 4, this period operates entirely on grid power (SSR = 0%), creating nighttime consumption peaks that significantly exceed the daytime loads of Mode 2. During the subsequent daytime (08:0011:00), the cooling demand is primarily satisfied by melting ice, causing the chillers to deactivate. With only minimal power load from auxiliary pumps remaining, the SSR hits 100%.

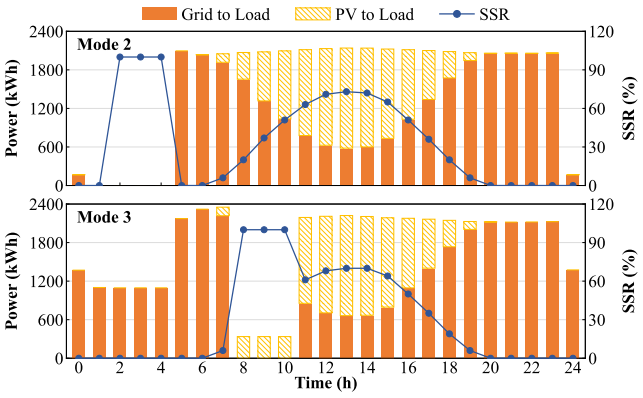


Figure 5. Dynamic electricity consumption breakdown and SSR on a typical high-load day.

Figure 6 compares the dynamic PV energy distribution and the SCR. Because the daytime electrical load perfectly

DOI
10.3384/ecp223371

matches the PV generation profile in Mode 2, almost all generated PV energy is consumpted by the active chillers, maintaining a 100% SCR from 07:00 to 19:00. Conversely, for Mode 3, the deactivation of chillers during the morning ice-discharging period results in a gap between the solar generation and the local load. The SCR plunges to a nadir of approximately 32% at 10:00, this mismatch causes substantial surplus PV energy to be exported to the grid, resulting in a waste of the PV self-consumption potential.

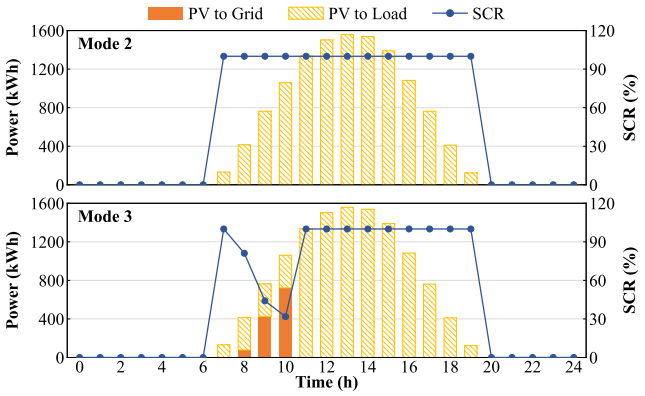


Figure 6. Dynamic PV utilization and SCR on a typical high-load day.

5.3 Economic Performance of the alternative operation modes

The economic performance of the three operation modes is detailed in Table 2.

Table 2. Comparison of annual economic performance under 3 modes.

Parameter	*Mode 1*	*Mode 2*	*Mode 3*
Grid electricity cost (CNY)			
Annual total	4,988,814	3,427,889	3,380,360
Change vs. Mode 1	–	−1,560,925	−1,608,454
Reduction	–	31.29%	32.24%
PV grid-export revenue (CNY)			
Annual total	1,054,136	424,970	528,702
Change vs. Mode 1	–	−629,166	−525,434
Reduction	–	59.69%	49.84%
Net operating cost (CNY)			
Annual total	3,934,678	3,002,919	2,851,658
Change vs. Mode 1	–	−931,759	−1,083,020
Reduction	–	23.68%	27.53%

The annual net operating cost is highest in Mode 1, at 3.9347 million CNY. By increasing the PV self-consumption rate, Mode 2 achieves a net cost reduction of 23.68%. However, Mode 3 exhibits the most superior economic benefits although it consumes more grid electricity than Mode 2. Its success stems from a strategy of electricity price arbitrage. By shifting the ice-storage energy to low-price nighttime, Mode 3 slashes the exorbitant cooling electricity expenses during daytime peaks. The effectiveness of this strategy is evident when comparing energy and cost reductions. The corresponding grid electricity cost plummets by 32.24% while grid electricity consumption is only reduced by 7.45% when compared to the baseline. While this mode accommodates a slightly lower 1.16 GWh of local PV self-consumption, the financial gains from load shifting outweigh the reduced PV utilization benefits. Ultimately, Mode 3 brings the annual net operating cost down to 2.8517 million CNY, achieving a maximized economic saving of 27.53% relative to the baseline. The results indicate that in a grid environment with significant peak-valley price spreads, the systems economic performance is not solely dependent on maximizing the PV self-consumption rate, but rather on an intelligent co-optimization of energy storage dispatch and TOU tariffs.

6 Conclusions

This study investigates the dispatch modes and economic response potential of a coupled PV and ITES air-conditioning system in a large high-speed railway station. The simulation model of the coupled system was constructed in MWorks by using the acausal Modelica language. The performance of three typical operation modes, including the independent PV grid-connection (Mode 1), PV self-consumption (Mode 2), and a dynamic mode combining PV direct supply with nighttime off-peak ice storage utilizing TOU tariffs (Mode 3), are analyzed and compared. The results demonstrate that Mode 3 is the optimal strategy for economic viability. Annual dynamic simulations confirm that, at the expense of a minor loss in physical energy efficiency, this mode utilizes deep tariff arbitrage to slash the baseline net operating cost from 3.9347 million CNY to 2.8517 million CNY, culminating in an impressive 27.53% economic saving. Additionally, this study verifies that it is effectiveness for evaluating the non-linear transient behaviors of complex multi-energy systems by using digital physical modelling combined with underlying hysteresis threshold controls and sequential dispatch logic. This study quantifies the economic response capacity of various dispatch modes to grid tariffs, and it is beneficial for the preliminary planning, flexible dispatch optimization, and investment decision-making of the coupled PV and ITES air-conditioning system in next-generation transportation hubs.

Acknowledgements

This work was supported by the Key Research and Development Project (Technology Innovation Program) of Hubei Provincial Science and Technology Plan (Grant number: 2025BCB033).

References

Chen, S., X. Zhou, Y. Yang, J. Li, S. Zhao, and J. Li (2025). "Modelica-based modeling and simulation of a novel dedi-

cated outdoor air-conditioning system with double heat recovery". In: *Journal of Building Engineering* 99, p. 111535. DOI: 10.1016/j.jobe.2024.111535.

Cirocco, L., P. Pudney, S. Riahi, R. Liddle, H. Semsarilar, J. Hudson, and F. Bruno (2022). "Thermal energy storage for industrial thermal loads and electricity demand side management". In: *Energy Conversion and Management* 270, p. 116190. DOI: 10.1016/j.enconman.2022.116190.

Dong, H., S. Vanage, and K. Cetin (2023). "Review of Ice Thermal Energy Storage (ITES) using Conventional Control Strategies in Commercial Buildings". In: *2023 ASHRAE Winter Conference*, p. 10. DOI: 10.63044/w23don61.

Fan, C. et al. (2021). "Open-source Modelica models for the control performance simulation of chiller plants with water-side economizer". In: *Applied Energy* 299, p. 117337. DOI: 10.1016/j.apenergy.2021.117337.

Formhals, J., X. Kirschstein, A. Dahash, L. Seib, and I. Sass (2024). "Development, validation and demonstration of a new Modelica pit thermal energy storage model for system simulation and optimization". In: *Geothermal Energy*. DOI: 10.1186/s40517-024-00302-9.

Hao, K., D. Kim, and J. E. Braun (2022). "Comparing the economic performance of ice storage and batteries for buildings with on-site PV through model predictive control and optimal sizing". In: *Journal of Building Performance Simulation* 15.5, pp. 691–715. DOI: 10.1080/19401493.2022.2084161.

Hillen, M., P. Schönfeldt, P. Groesdonk, and B. Hoffschmidt (2025). "Operational Optimization of Seasonal Ice-Storage Systems with Time-Series Aggregation". In: *Energies* 18.22, p. 5988. DOI: 10.3390/en18225988.

Hinkelman, K., J. Wang, W. Zuo, A. Gautier, M. Wetter, C. Fan, and N. Long (2022). "Modelica-based modeling and simulation of district cooling systems: A case study". In: *Applied Energy* 311, p. 118654. DOI: 10.1016/j.apenergy.2022.118654.

Li, G., Y. Fu, A. Pertzborn, J. Wen, and Z. O'Neill (2021). "An Ice Storage Tank Modelica Model: Implementation and Validation". In: pp. 177–185. DOI: 10.3384/ecp21181177.

Lu, X., Y. Fu, Z. O'Neill, and J. Wen (2021). "A holistic fault impact analysis of the high-performance sequences of operation for HVAC systems: Modelica-based case study in a medium-office building". In: *Energy and Buildings* 252, p. 111448. DOI: 10.1016/j.enbuild.2021.111448.

Menezes, M. V. P., A.-H. Othman, J. Tancabel, and V. C. Aute (2026). "An approach for fast and accurate simulation of phase change material based thermal energy storage in buildings". In: *Journal of Energy Storage* 152, p. 120384. DOI: 10.1016/j.est.2026.120384.

Onaolapo, A. K., R. P. Carpanen, D. G. Dorrell, and E. E. Ojo (2021). "Reliability Evaluation and Financial Viability of an Electricity Power Micro-Grid System With the Incorporation of Renewable Energy Sources and Energy Storage: Case Study of KwaZulu-Natal, South Africa". In: *IEEE Access* 9, pp. 159908–159924. DOI: 10.1109/ACCESS.2021.3129980.

Pinamonti, M., A. Prada, and P. Baggio (2020). "Rule-Based Control Strategy to Increase Photovoltaic Self-Consumption of a Modulating Heat Pump Using Water Storages and Building Mass Activation". In: *Energies* 13.23, p. 6282. DOI: 10.3390/en13236282.

Shi, Z., W. Wang, Y. Huang, P. Li, and L. Dong (2022). "Simultaneous optimization of renewable energy and energy storage capacity with hierarchical control". In: *CSEE Journal of Power and Energy Systems* 8.1, pp. 95–104. DOI: 10.17775/CSEEJPES.2019.01470.

Tang, H., J. Yu, Y. Geng, X. Liu, and B. Lin (2023). "Optimization of operational strategy for ice thermal energy storage in a district cooling system based on model predictive control". In: *Journal of Energy Storage* 62, p. 106872. DOI: 10.1016/j.est.2023.106872.

Wetter, M., W. Zuo, T. S. Nouidui, and X. Pang (2014). "Modelica Buildings library". In: *Journal of Building Performance Simulation* 7.4, pp. 253–270. DOI: 10.1080/19401493.2013.765506.

Zhu, H., H. Li, G. Liu, Y. Ge, J. Shi, H. Li, and N. Zhang (2023). "Energy storage in Variable high renewable penetration power systems: Technologies, applications, supporting policies and suggestions". In: *CSEE Journal of Power and Energy Systems* 9.6, pp. 2099–2108. DOI: 10.17775/CSEEJPES.2020.00090.